Enhancing imaging systems using transformation optics

David R. Smith[1,*] Yaroslav Urzhumov,[1] Nathan B. Kundtz,[1, 2] and Nathan I. Landy[1]

[1]*Center for Metamaterials and Integrated Plasmonics and Department of Electrical and Computer Engineering, Duke University, Box 90291, Durham, NC 27708, USA*
[2]*Intellectual Ventures, 3150 139th Ave SE Building, Bellevue, WA 98005, USA*
**drsmith@ee.duke.edu*

Abstract: We apply the transformation optical technique to modify or improve conventional refractive and gradient index optical imaging devices. In particular, when it is known that a detector will terminate the paths of rays over some surface, more freedom is available in the transformation approach, since the wave behavior over a large portion of the domain becomes unimportant. For the analyzed configurations, quasi-conformal and conformal coordinate transformations can be used, leading to simplified constitutive parameter distributions that, in some cases, can be realized with isotropic index; index-only media can be low-loss and have broad bandwidth. We apply a coordinate transformation to flatten a Maxwell fish-eye lens, forming a near-perfect relay lens; and also flatten the focal surface associated with a conventional refractive lens, such that the system exhibits an ultra-wide field-of-view with reduced aberration.

OCIS codes: (160.3918) Metamaterials; (120.4570) Optical design of instruments; (230.0230) Optical devices; (220.3630) Lenses; (220.3620) Lens system design; (110.2760) Gradient-index lenses.

References and links

1. J. B. Pendry, D. Schurig, and D. R. Smith, "Controlling electromagnetic fields," Science **312**(5781), 1780–1782 (2006).
2. E. G. Post, Formal Structure of Electromagnetics: General Covariance and Electromagnetics (Interscience Publishers, New York, 1962).
3. A. Nicolet, J. F. Remacle, B. Meys, A. Genon, and W. Legros, "Transformation methods in computational electromagnetism," J. Appl. Phys. **75**(10), 6036–6038 (1994).
4. A. J. Ward, and J. B. Pendry, "Refraction and geometry in Maxwell's equations," J. Mod. Opt. **43**, 773–793 (1996).
5. D. Schurig, J. J. Mock, B. J. Justice, S. A. Cummer, J. B. Pendry, A. F. Starr, and D. R. Smith, "Metamaterial electromagnetic cloak at microwave frequencies," Science **314**(5801), 977–980 (2006).
6. R. Liu, C. Ji, J. J. Mock, J. Y. Chin, T. J. Cui, and D. R. Smith, "Broadband ground-plane cloak," Science **323**(5912), 366–369 (2009).
7. V. M. Shalaev, "Physics. Transforming light," Science **322**(5900), 384–386 (2008).
8. U. Leonhardt, and T. G. Philbin, "General relativity in electrical engineering," N. J. Phys. **8**(10), 247 (2006).
9. D. A. Genov, S. Zhang, and X. Zhang, "Mimicking celestial mechanics in metamaterials," Nat. Phys. **5**(9), 687–692 (2009).
10. D. A. Roberts, N. Kundtz, and D. R. Smith, "Optical lens compression via transformation optics," Opt. Express **17**(19), 16535–16542 (2009).
11. D.-H. Kwon, D. H. Werner, "Transformation optical designs for wave collimaters, flat lenses and right-angle bends," N. J. Phys. **10**(11), 115023 (2008).
12. D. H. Kwon, D. H. Werner; "Flat focusing lens designs having minimized reflection based on coordinate transformation techniques," Opt. Express **17**(10), 7807–7817 (2009).
13. D. Schurig, "An aberration-free lens with zero *f*-number," N. J. Phys. **10**(11), 115034 (2008).
14. N. Kundtz, and D. R. Smith, "Extreme-angle broadband metamaterial lens," Nat. Mater. **9**(2), 129–132 (2010).
15. Y. G. Ma, C. K. Ong, T. Tyc, and U. Leonhardt, "An omnidirectional retroreflector based on the transmutation of dielectric singularities," Nat. Mater. **8**(8), 639–642 (2009).
16. J. Li, and J. B. Pendry, "Hiding under the carpet: a new strategy for cloaking," Phys. Rev. Lett. **101**(20), 203901 (2008).

#132121 - $15.00 USD Received 23 Jul 2010; revised 14 Sep 2010; accepted 15 Sep 2010; published 22 Sep 2010

17. J. Valentine, J. Li, T. Zentgraf, G. Bartal, and X. Zhang, "An optical cloak made of dielectrics," Nat. Mater. **8**(7), 568–571 (2009).
18. L. H. Gabrielli, J. Cardenas, C. B. Pointras, and M. Lipson, "Silicon nanostructure cloak operating at optical frequencies," Nat. Photonics **3**(8), 461 (2009).
19. T. Ergin, N. Stenger, P. Brenner, J. B. Pendry, and M. Wegener, "Three-dimensional invisibility cloak at optical wavelengths," Science **328**(5976), 337–339 (2010).
20. E. W. Marchand, Gradient Index Optics (Academic Press, New York, 1978).
21. D. Schurig, J. B. Pendry, and D. R. Smith, "Calculation of material properties and ray tracing in transformation media," Opt. Express **14**(21), 9794–9804 (2006).
22. U. Leonhardt, "Optical conformal mapping," Science **312**(5781), 1777–1780 (2006).
23. N. I. Landy, and W. J. Padilla, "Guiding light with conformal transformations," Opt. Express **17**(17), 14872–14879 (2009).
24. P. Knupp, and S. Steinberg, Fundamentals of Grid Generation (CRC Press, Boca Raton, FL, 1993).
25. Z. Chang, X. Zhou, J. Hu, and G. Hu, "Design method for quasi-isotropic transformation materials based on inverse Laplace's equation with sliding boundaries," Opt. Express **18**(6), 6089–6096 (2010).
26. N. B. Kundtz, Advances in Complex Artificial Electromagnetic Media, PhD Dissertation, Duke University, Durham, N. Carolina (2009).
27. S. A. Cummer, B. I. Popa, D. Schurig, D. R. Smith, and J. Pendry, "Full-wave simulations of electromagnetic cloaking structures," Phys. Rev. E Stat. Nonlin. Soft Matter Phys. **74**(3), 036621 (2006).
28. E. Hecht, Optics, 4th Ed. (Addison-Wesley, San Francisco, 2002).

1. Introduction

Transformation optics (TO) is a recently appreciated design approach for electromagnetic and optical materials [1]. In TO, geometry and coordinate transformations play the dominant role in the design process, in a manner analogous to ray-tracing in geometrical optics. TO proceeds from the observation that Maxwell's equations can be written in a form-invariant manner regardless of the system of coordinates used, provided that the tensor elements of the constitutive parameters (i.e., the electric permittivity and magnetic permeability) are allowed to become functions of the spatial coordinates. Although the form invariance of Maxwell's equations has long been known [2], and has been applied in various numerical simulation schemes [3,4], using TO as a means of designing actual optical devices is a much newer pursuit. Initially proposed as a means to design exotic structures such as "invisibility cloaks" or "optical black holes" [5–9], TO has also emerged as a general tool for optical design that can be applied to enhance the properties of conventional optical devices [10–15].

In the TO method, a coordinate transformation is applied to a region of space that can either be empty, or may contain an object in the form of a spatial distribution of constitutive parameters. If a solution to the wave equation is found using a particular coordinate system, a coordinate transformation cannot change this underlying wave solution; thus, if the wave solution is expressed in a different set of coordinates and plotted in the new coordinate system, it will appear identical to the original field distribution. However, if the *transformed* field distribution is viewed relative to the *original* coordinate system, it will appear distorted. By judiciously choosing coordinate transformations such that a field pattern is distorted or modified in some desired manner, an optical device can be intuitively designed. By subsequently applying the coordinate transformation to the constitutive tensors in a manner suggested by the form-invariance of Maxwell's equations, the specification of a medium is obtained that will physically distort the waves exactly as the coordinate transformation predicts. By implementing the specified constitutive parameters using metamaterials or other means, the transformation optical device transitions from virtual to actual.

Materials designed by the TO method are inherently complex. An arbitrary coordinate transformation typically results in a medium that is anisotropic and with both permittivity and permeability tensor elements that vary independently throughout space. Such media are akin to gradient index (GRIN) media, though considerably more demanding. In fact, the material properties of TO media are often so extreme—many designs have constitutive parameter values that tend to zero or infinity—that they would likely be dismissed as impractical. Fortunately, over the past decade, structured metamaterials have shown promise as a means of achieving extreme material properties. The constitutive properties of a metamaterial can be

#132121 - $15.00 USD Received 23 Jul 2010; revised 14 Sep 2010; accepted 15 Sep 2010; published 22 Sep 2010

carefully designed and controlled, allowing for precise spatial gradients to be introduced into a medium in either the permittivity or permeability elements. The combination of metamaterials and the TO design approach have allowed new optical design strategies to surface.

One method of leveraging the TO approach for optical design is to start with an optical device that performs some function—such as focusing or collimating rays—and transforming the geometry so that the device has more advantageous features. Transformations have been used, for example, to illustrate how the profile of a conventional refractive lens might be reduced [10] or how a spherical Luneburg GRIN lens might be flattened [14]. In this paper we build on these prior approaches, showing two optical devices that can be derived by modifying existing imaging elements, guided by first performing coordinate transformations. We show that the TO methodology allows an intuitive design procedure that holds the potential for greatly improved imaging systems.

While we are not concerned with the ultimate implementation of the proposed devices here, we note that the modification of a geometry can be accomplished with an infinite number of potential coordinate transformations—some exact and some approximate—so that we have the opportunity to apply optimization techniques to arrive at much more achievable material properties. An important type of optimization was introduced by Li and Pendry [16], who suggested the use of a numerical scheme to achieve quasi-conformal transformations. These numerical methods seek transformations that minimize the anisotropy of the constitutive tensors and, at least in two-dimensional geometries, can produce index-only TO designs that have small absorption and broad bandwidth. After the introduction of the quasi-conformal approach, numerous quasi-conform transformation optical (QCTO) devices were rapidly demonstrated, many of them scaling to telecommunications and visible wavelengths [6, 14, 17–19]. In this paper we describe the QCTO approach and apply it to reduce the anisotropy associated with the configurations considered.

2. The flattened Maxwell fish-eye lens

There are a number of optical devices that have advantageous imaging properties, but are inconvenient to use due to their form factors or necessary index distributions. In particular, several classes of spherically symmetric GRIN lenses exist that can focus rays without any geometrical aberrations [10, 14, 15]. The Luneburg lens is representative of this class, having an index distribution that varies radially and that focuses rays from infinity to points on the surface of a sphere. Schurig proposed a set of transformations that would effectively flatten the Luneburg lens [10], possibly allowing it to be utilized with a planar detector array while retaining its advantageous aberration-free imaging characteristics and ultra-wide field-of-view. The flattening of the Luneburg using TO is possible because the focal surface coincides directly with the Luneburg surface; thus, the rays or fields that extend beyond the transformed focal surface are of no importance, since it is assumed that all rays will terminate on a detector array.

The termination of rays on a detector plane can be used in many other contexts to similarly improve or modify exist optical devices. For example, the Maxwell fish-eye lens is another GRIN device formed from a radial distribution of index that varies as

$$n(r) = \frac{n_0}{1 + (r/a)^2} \tag{1}$$

where n_0 is the index-of-refraction at the center of the lens and a is the radius of the lens [20]. The fish-eye lens focuses rays emanating from a point on the lens surface to a conjugate point on the opposite side of the lens. All pairs of object and image points are aplanatic, thus the fish-eye lens is a perfect imaging instrument; however, the curved object and image surfaces generally make the fish-eye lens more a curiosity rather than a useful device. By

#132121 - $15.00 USD Received 23 Jul 2010; revised 14 Sep 2010; accepted 15 Sep 2010; published 22 Sep 2010

applying a transformation that flattens two sides of the lens, it may be possible to increase the utility of the fish-eye, for use, say, as a perfect relay lens.

The properties of GRIN optics, at least in the geometrical optics limit, are easily accessible utilizing standard ray tracing techniques. To determine ray trajectories for Eq. (1) and the other configurations described here, we assume the ray trajectory is parameterized by the path length, s, such that

$$\frac{d}{ds}\left(n(\mathbf{q})\frac{dq_i}{ds} \right) = \frac{dn}{dq_i}, \tag{2}$$

where i indexes the general coordinate q_i [20]. Equations (2) can be integrated to find the path of a ray through a medium with an arbitrary (but isotropic) index distribution, the position and direction of the ray serving as sufficient initial conditions. Applying Eqs. (2) to the index distribution in Eq. (1), we numerically integrate a series of rays using the NDSolve function in Mathematica (Wolfram), obtaining the well-known behavior shown in Fig. 1a.

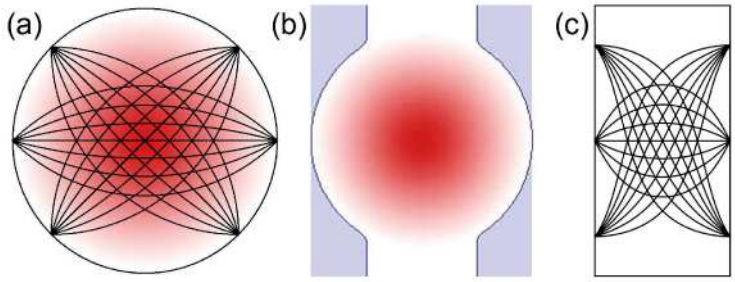

Fig. 1. (a) The Maxwell fish-eye lens is a perfect optical instrument, connecting pairs of aplanatic points on one side of the sphere to the other. The fish-eye lens has a radial distribution of index, given by Eq. (1). (b) Since both image and object points lie on the sphere with the rays contained within the medium, the boundary conditions on the surface are immaterial. We can, for example, imagine two sides terminated by conducting boundary conditions, as illustrated in the figure. The boundary and the interior region can then be transformed. (c) Utilizing the transformation provided in Eq. (3), the fish-eye lens can be flattened to form a perfect relay lens.

The fish-eye lens can be flattened using the coordinate transformation

$$\begin{aligned} x'(x,z) &= \frac{w}{a}x \\ z'(x,z) &= \frac{z\,l}{\sqrt{a^2 - x^2}}, \end{aligned} \tag{3}$$

which maps a cylindrical region of radius a into a rectangular region of width w and height l [11]. We need only transform the sphere region, since we are not concerned with rays beyond either the object or the image points. The expected behavior of the transformed medium can be immediately obtained by plotting the ray trajectories computed for the untransformed fish-eye using the transformed coordinates of Eqs. (3), as described in the introduction. The result is shown in Fig. 1c, where we see that the spherical region has been mapped to a rectangle, such that the sources and their images lie on planar boundaries. The transformed device thus acts as a perfect relay lens, translating a distribution of sources over a distance with zero geometrical aberrations. For the transformation, we have arbitrarily chosen $l = a/2$ and $w = a$, a geometry that will be used throughout for the fish-eye geometry. The permittivity and permeability tensors needed to achieve the behavior shown in Fig. 1c can be found from the usual TO prescription [21] as

#132121 - $15.00 USD Received 23 Jul 2010; revised 14 Sep 2010; accepted 15 Sep 2010; published 22 Sep 2010

$$\varepsilon' = \frac{\Lambda \varepsilon \Lambda^T}{|\Lambda|} n^2(x,z)$$
$$\mu' = \frac{\Lambda \mu \Lambda^T}{|\Lambda|}, \tag{4}$$

Where $n(x,z)$ is the initial index distribution, in this case corresponding to the fish-eye lens. The tensor Λ is the Jacobian matrix relating differential distances between the two coordinate systems, and has the explicit form

$$\Lambda = \begin{pmatrix} \frac{\partial x'}{\partial x} & \frac{\partial x'}{\partial y} & \frac{\partial x'}{\partial z} \\ \frac{\partial y'}{\partial x} & \frac{\partial y'}{\partial y} & \frac{\partial y'}{\partial z} \\ \frac{\partial z'}{\partial x} & \frac{\partial z'}{\partial y} & \frac{\partial z'}{\partial z} \end{pmatrix} \tag{5}$$

While we could evaluate the elements of Λ using the transformation of Eqs. (2), the resulting medium would not be a practical realization, and the effort of writing down the transformation explicitly would not be illuminating. We instead make use of the quasi-conformal TO method to arrive at a numerical transformation that leads to more realistic material parameters. We describe the QCTO method in the following section.

3. Quasi-conformal transformations

The transformation of Eq. (3) is convenient because it is analytic and conceptually simple; however, it leads to material parameters that are extreme. Fortunately, the geometry of the fish-eye is such that we can employ an optimization technique, in which the anisotropy of the material parameters is minimized. It has been shown that the scalar two dimensional Helmholtz equation is form-invariant for coordinate transformations that equate to conformal mappings [22]. Such transformations are advantageous in that the required media can be realized with isotropic, graded refractive index; though analytic mappings are not always possible to find for a given set of boundary conditions. For general boundary conditions, a quasi-conformal transformation optics (QCTO) technique can be applied that produces an approximate transformation that minimizes anisotropy and the need for magnetic response. Depending on the nature of the boundary conditions, the optimized transformation can be exactly conformal if the virtual and physical spaces have the same conformal module [23]. We now briefly summarize the steps utilized in the QCTO method.

If we consider a transformation that lies within the x-y plane, and assume a polarization such that the electric field is polarized along the z-axis, then the Jacobian matrix (Eq. (5) reduces to

$$\Lambda = \begin{pmatrix} \frac{\partial x'}{\partial x} & \frac{\partial x'}{\partial y} & 0 \\ \frac{\partial y'}{\partial x} & \frac{\partial y'}{\partial y} & 0 \\ 0 & 0 & 1 \end{pmatrix}, \tag{6}$$

and the constitutive tensor for the permittivity becomes

#132121 - $15.00 USD Received 23 Jul 2010; revised 14 Sep 2010; accepted 15 Sep 2010; published 22 Sep 2010

$$\varepsilon = \frac{1}{\frac{\partial x'}{\partial x}\frac{\partial y'}{\partial x} - \frac{\partial y'}{\partial x}\frac{\partial x'}{\partial y}} \begin{pmatrix} \left(\frac{\partial x'}{\partial x}\right)^2 + \left(\frac{\partial x'}{\partial y}\right)^2 & \frac{\partial x'}{\partial x}\frac{\partial y'}{\partial x} + \frac{\partial x'}{\partial y}\frac{\partial y'}{\partial y} & 0 \\ \frac{\partial x'}{\partial x}\frac{\partial y'}{\partial x} + \frac{\partial x'}{\partial y}\frac{\partial y'}{\partial y} & \left(\frac{\partial y'}{\partial y}\right)^2 + \left(\frac{\partial y'}{\partial x}\right)^2 & 0 \\ 0 & 0 & 1 \end{pmatrix}. \tag{7}$$

To ensure that the off-diagonal elements are zero, it is required that

$$\frac{\partial x'}{\partial x}\frac{\partial y'}{\partial x} = -\frac{\partial x'}{\partial y}\frac{\partial y'}{\partial y}. \tag{8}$$

At this point it is convenient to introduce a function that will serve to measure the degree of anisotropy of the transformation everywhere throughout space. We define a function $f(x, y)$ such that

$$f\frac{\partial x'}{\partial x} = \frac{\partial y'}{\partial y}; \tag{9}$$

using Eq. (8), we find furthermore that

$$-\frac{1}{f}\frac{\partial y'}{\partial x} = \frac{\partial x'}{\partial y}. \tag{10}$$

Equations (9) and 10 are known as the Beltrami equations [23, 24]. It can be seen by inspection of Eqs. (7), 9 and 10 that if $f = 1$ everywhere, the medium will be isotropic in the plane (i.e., off-diagonal elements equal to zero, in-plane diagonal elements equal to each other). Under this condition, Eqs. (9) and 10 reduce to the Cauchy-Riemann equations, indicating the coordinate transformation is a conformal map. By taking another derivative and noting that the partial derivatives commute, we find the following set of equations:

$$\begin{aligned} \frac{\partial}{\partial x} f\frac{\partial x'}{\partial x} + \frac{\partial}{\partial y} f\frac{\partial x'}{\partial y} = 0 \\ \frac{\partial}{\partial x}\frac{1}{f}\frac{\partial y'}{\partial x} + \frac{\partial}{\partial y}\frac{1}{f}\frac{\partial y'}{\partial y} = 0. \end{aligned} \tag{11}$$

We can find the explicit form for $f(x, y)$ from Eqs. (9) and 10, which yield

$$\left(\frac{\partial x'}{\partial x}\right)^2 + \left(\frac{\partial x'}{\partial y}\right)^2 = \frac{1}{f^2}\left[\left(\frac{\partial y'}{\partial y}\right)^2 + \left(\frac{\partial y'}{\partial x}\right)^2\right], \tag{12}$$

or, equivalently [25],

$$f = \sqrt{\frac{\left(\frac{\partial y'}{\partial y}\right)^2 + \left(\frac{\partial y'}{\partial x}\right)^2}{\left(\frac{\partial x'}{\partial x}\right)^2 + \left(\frac{\partial x'}{\partial y}\right)^2}}. \tag{13}$$

#132121 - $15.00 USD Received 23 Jul 2010; revised 14 Sep 2010; accepted 15 Sep 2010; published 22 Sep 2010

Equation (13) is the ratio of the in-plane permittivity or permeability elements; and, when combined with Eqs. (11), Eq. (13) yields a set of nonlinear partial differential equations that can be solved for $x'(x, y)$ and $y'(x, y)$. As noted above, should we desire to minimize the anisotropy associated with the transformation, we should seek a solution to the equations with $f = 1$. If such a solution were available, Eq. (11) would reduce to Laplace's equations, i.e.

$$\frac{\partial^2 x'}{\partial x^2} + \frac{\partial^2 y'}{\partial y^2} = 0$$
$$\frac{\partial^2 y'}{\partial x^2} + \frac{\partial^2 y'}{\partial y^2} = 0, \tag{14}$$

with Eqs. (9) and 10 reducing to the Cauchy-Riemann conditions of holomorphic function theory. A transformation that satisfies both sets of equations is inherently conformal. In general, however, conformal solutions cannot be found for arbitrary geometries, and our best general procedure is to attempt to solve the equations numerically to find a quasi-conformal solution, realizing that there will be some residual error leading to some anisotropy throughout the optimized medium. Our goal is that the residual error be small enough that it can be neglected in the final design.

To solve the equations, we must apply boundary conditions everywhere on the region bounding the transformation, typically a combination of Neumann-Dirichlet boundary conditions at surfaces known to be terminated by a detector array or generalized caustic surface, and Dirichlet boundary conditions where the transformation connects to free space. The Neumann-Dirichlet boundary conditions allow the transformation grid to "slip" along the boundary during the iterative optimization process, while the Dirichlet boundary condition forces points on the boundary to remain fixed. For the fish-eye lens transformation to be described below, either a combination of boundary conditions could be used, or Neumann-Dirichlet boundary conditions could be used on all surfaces in a manner that would lead to a fully conformal mapping [23–25]. Both sets of boundary conditions were attempted, with little variation found in the final index distribution. Note that there will be some error associated with any quasi-conformal versus conformal map, but the error may be very small for practical situations.

3. Quasi-conformal transformation for the fish-eye lens

To illustrate the quasi-conformal technique, we perform the optimization described in the previous section, starting with the arbitrary initial mesh illustrated in Figs. 2. To obtain the mesh, an initial rectangular grid was patterned over the rectangular region representing the virtual space, and the grid deformed progressively such that the grid lines at the minimum and maximum y-values in the virtual space conformed to the circular boundary of the fish-eye (physical space). The x-values are not changed by the initial transformation ($x' = x$). Note that the "squareness" (orthogonality) of the grid is lost in the spherical central region, indicating the equivalent material parameters will exhibit significant anisotropy. The anisotropy can be displayed by computing the tensor elements of the permittivity using Eq. (4). We see from Fig. 2 that the diagonal elements of the permittivity tensor have values ranging from below unity to some finite value greater than unity, while the off-diagonal elements have finite (positive and negative) values. Though the medium specified by this transformation will in principle serve to flatten the fish-eye lens, its material properties would be very difficult to achieve in practice.

#132121 - $15.00 USD Received 23 Jul 2010; revised 14 Sep 2010; accepted 15 Sep 2010; published 22 Sep 2010

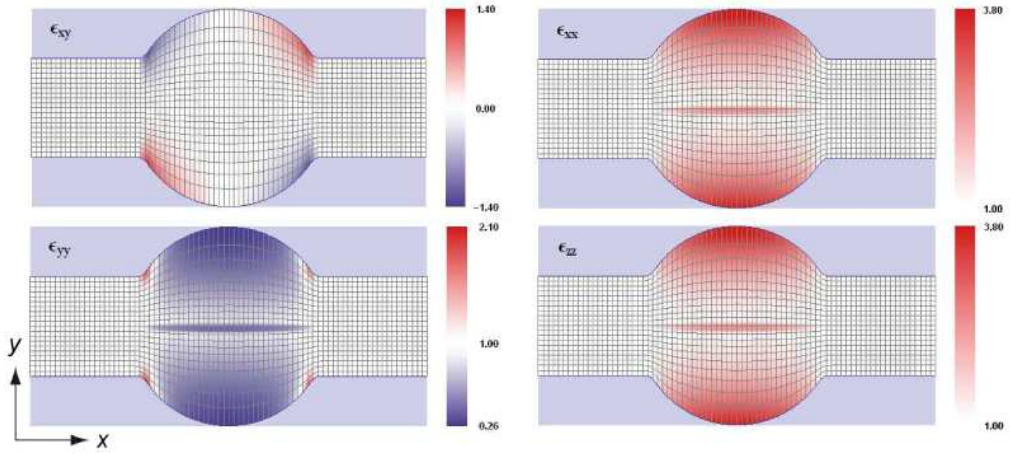

Fig. 2. The spatial grid and the components of the dielectric permittivity tensor for the transformation that flattens a cylindrical region. The central region is in the shape of a cylinder with radius $a = 1$ (arbitrary units). The shaded areas above and below the grids indicate regions of perfect electric conductor (PEC). The plotted regions extend from $x = -2a$ to $x = +2a$ along the *x*-axis, and from $y = -a/2$ to $y = +a/2$ along the *y*-axis (outside of the cylindrical region).

As an alternative to the grid shown in Fig. 2, we can attempt to search for a solution that satisfies Eqs. (14), at least approximately. Starting with the grid shown in Fig. 2 as an initial guess, and solving Eqs. (14) numerically in Mathematica using a standard relaxation method [26], we arrive at the grid shown in Fig. 3. Note the orthogonality of the mesh, which indicates that the anisotropy of the medium has been minimized. The corresponding constitutive parameters also reveal that of the diagonal elements, only ε_{zz} is significant, except near the corners of the transformation. Since we do not expect fields to sample this region with much weight, neglecting this anisotropy is justified. Elsewhere, the in-plane diagonal elements are near unity and the off-diagonal elements are close to zero. The out-of-plane component, ε_{zz}, ranges from unity to a value of nearly eight.

In both Figs. 2 and 3 we have plotted the transformation grid in the physical space, yet overlaid the constitutive parameters corresponding to the virtual space, where the cylindrical region has been flattened. This choice of representation is a convenience here, as it allows us to show the initial grid and the material parameters in the same plot. It is also possible to plot the physical space grid in the virtual frame via interpolation of the coordinate transformation and contour plotting. The inverse transformation is illustrated by the grid lines in Fig. 4 for the optimized, QCTO mesh. We show only the ε_{zz} distribution, since in the final design we expect to neglect the anisotropy of the other components. The final distribution of ε_{zz} is greater than or equal to unity nearly everywhere except near the sharp corners where the circular arc connects to the plane. This region, however, is relatively small and can be set to unity without significant degradation of the solutions of interest.

Once the transformation grid has been determined, we have a means of flattening the space between two cylindrical surfaces. Since, for the fish-eye, the cylindrical region possesses a distribution of index according to Eq. (1), we can simply multiply the transformation permittivity distribution by the square of the fish-eye index distribution to arrive at a medium that will function as a flattened fish-eye. The distribution for the empty space transformation is shown in Fig. 4a, the distribution for the fish-eye in Fig. 1b, and the composite distribution shown in Fig. 4b. To obtain the index distribution for the fish-eye, we arbitrarily set $n_0 = 2$ in Eq. (1).

#132121 - $15.00 USD Received 23 Jul 2010; revised 14 Sep 2010; accepted 15 Sep 2010; published 22 Sep 2010

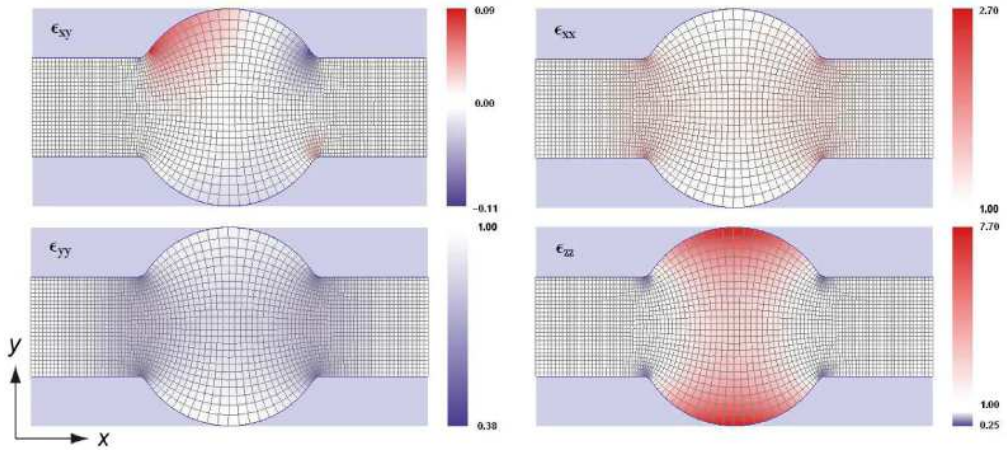

Fig. 3. The spatial grid and the components of the dielectric permittivity tensor for the *quasi-conformal* transformation that flattens a cylindrical region. The central region is in the shape of a cylinder with radius $a = 1$ (arbitrary units). The shaded areas above and below the grids indicate regions of perfect electric conductor (PEC). The plotted regions extend from $x = -2a$ to $x = +2a$ along the *x*-axis, and from $y = -a/2$ to $y = +a/2$ along the *y*-axis (outside of the cylindrical region).

With the final index distribution in hand, we can test whether or not the neglect of the other components is justified. In Fig. 5a, we present a ray trace through the inhomogeneous index distribution presented in Fig. 4b. The same three sources are used as in Fig. 1c, and Eqs. (2) integrated to determine the trajectories. Figure 5a shows nearly the identical focusing properties as predicted by the full transformation in Fig. 1c. The distribution of index values lies between roughly unity and ~3.5, which should be obtainable utilizing electric, non-resonant metamaterials. As has been shown [6, 14, 17, 18], such metamaterials can be used to form low-loss, broadband structures that scale well towards visible wavelengths. The flattened fish-eye lens shown here could thus function as a relay lens with considerable efficiency.

We can further confirm the performance of the flattened fish-eye with numerical simulations using COMSOL, a full-wave EM solver based on the Finite Element Method. The use of COMSOL to evaluate TO structures has been described previously [27]. The results of full-wave simulations assuming a two-dimensional geometry in which the electric field is polarized out of the plane of propagation (i.e., transverse electric, or TE polarization) are shown in Figs. 5b and 5c. The source of excitation is a line source consisting of an out-of-plane electric current. In Fig. 5b, the line source is placed on the optical axis and, in Fig. 5c, the line source is offset by a quarter of the original fish-eye radius, a —thus, one half of the flattened lens thickness. The free space above and below the lens is gradually terminated with perfectly matched layers of refractive index n = 1. The simulations in Figs. 5b and 5c demonstrate the expected focusing behavior. Similar TE-wave focusing behavior was observed with point magnetic dipole sources oriented either vertically or horizontally in the plane of propagation (not shown).

#132121 - $15.00 USD Received 23 Jul 2010; revised 14 Sep 2010; accepted 15 Sep 2010; published 22 Sep 2010

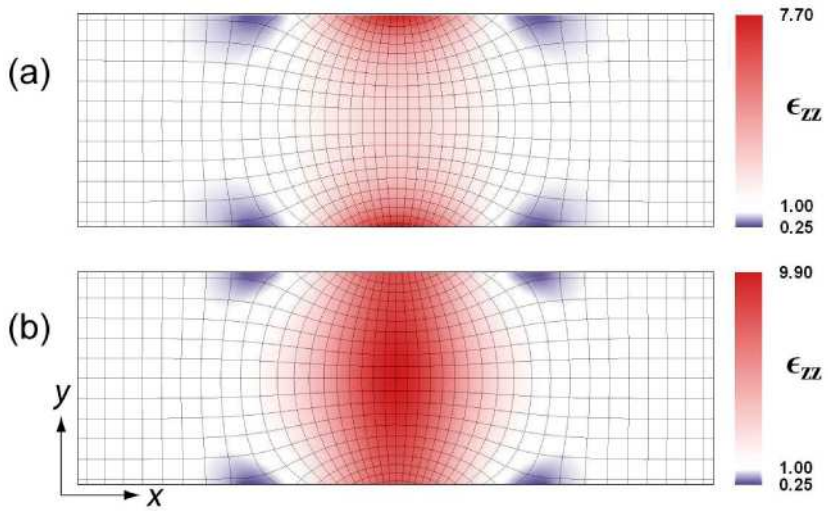

Fig. 4. (a) Permittivity distribution in the virtual frame, shown with grid lines representing the inverse transformation. This transformation assumes the interior region to be flattened consists only of free space. (b) Permittivity distribution corresponding to the coordinate transformation combined with the fish-eye permittivity distribution of Eq. (1) (with $n_0 = 2$). This distribution corresponds to the flattened fish-eye. The plotted regions extend from $x = -2a$ to $x = +2a$ along the x-axis, and from $y = -a/2$ to $y = +a/2$ along the y-axis, where a corresponds to the original fish-eye lens radius.

In the geometrical optical limit, there should be no difference between TE and TM (transverse magnetic) polarizations. To test the lens performance with respect to TM polarization, the index distribution was made isotropic (i.e., ε_{xx} and ε_{yy} set equal to ε_{zz}), and magnetic line sources (fictitious out-of-plane magnetic current) used to demonstrate imaging of a "monopole" point source. The resulting field plots, shown in Figs. 5d and 5e, reveal the solution works for TM waves as anticipated. Similar results (not shown) were obtained for imaging of point electric dipoles oriented arbitrarily in the plane of the lens.

#132121 - $15.00 USD Received 23 Jul 2010; revised 14 Sep 2010; accepted 15 Sep 2010; published 22 Sep 2010

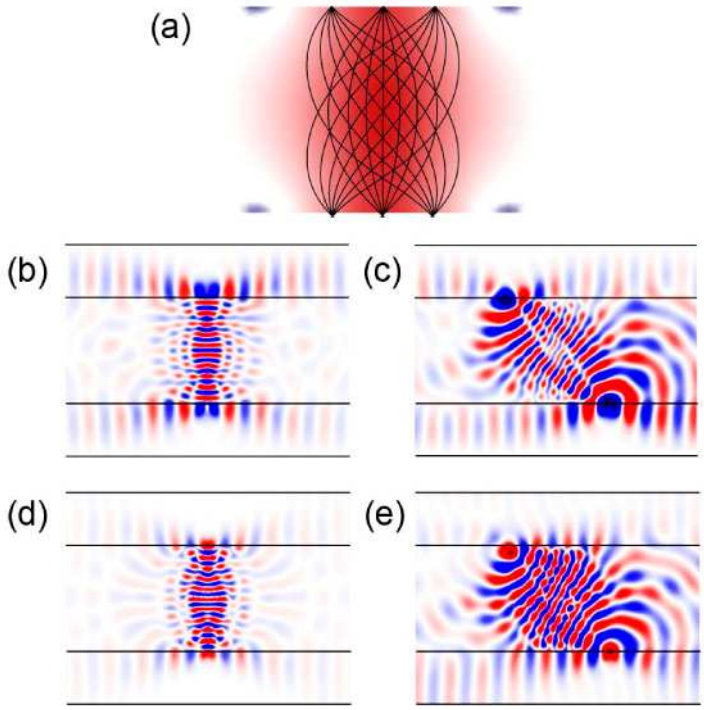

Fig. 5. Numerical simulations of the flattened fish-eye lens of thickness a. (a) Ray tracing calculation showing three pencils originating from the bottom surface of the lens, on and off (shifted + 0.5a and –0.5a from the center) the optical axis. (b) Full-wave TE-polarization simulations of the same system with a point source located at the bottom surface on the optical axis. The free-space wavelength is 0.3a. Color shows the out-of-plane electric field. (c) Same as (b) but the source is shifted off-axis by 0.5a. (d) Same as (b) but with TM-polarization excitation; color shows out-of-plane magnetic field. (e) Same as (d), but with off-axis displacement 0.5a. In all cases, the interior region corresponding to the lens extends from $x = -2a$ to $x = +2a$ along the horizontal axis, and from $y = -a/2$ to $y = +a/2$ along the vertical axis.

4. Compensation of field curvature using transformation optics

In any imaging situation where it is known that a detector array will terminate ray trajectories, TO approaches can be conveniently applied. As an additional example, we illustrate the flattening of the focal surface corresponding to a conventional refractive lens. The geometry is shown in Fig. 6a, where we present a standard ray diagram of a lens focusing rays incident from infinity at several angles. The index of the lens is $n = 2$. The lens surfaces are cylindrical, defined by the equation

$$\frac{\left(z - R_i - V_i\right)^2}{R_i^2} + \frac{x^2}{R_i^2} = 1, \tag{15}$$

where the z-axis is assumed to be the optical axis and i indexes the two lens surfaces. For the lens shown, the radii of the two surfaces are $R_1 = +15\,mm$ and $R_2 = +45\,mm$, with vertices at $V_1 = 0\,mm$ and $V_2 = 2\,mm$. The diameter of the lens is $D = 13\,mm$.

The imaging properties of refractive lenses are impacted by their inherent aberration profile. The lowest order Seidel aberrations include spherical aberration, coma, field curvature, distortion and astigmatism [28]. In practice, one or more of the aberrations can be minimized by "bending" the lens—that is, choosing a ratio of the front-to-back radii of

#132121 - $15.00 USD Received 23 Jul 2010; revised 14 Sep 2010; accepted 15 Sep 2010; published 22 Sep 2010

curvature of the lens surfaces that optimizes the lens for a given application. However, it is not possible to simultaneously eliminate all of the aberrations; in particular, the field-of-view of a lens may be limited by its field curvature aberration, which becomes increasingly difficult to minimize while simultaneously minimizing the other aberrations.

For the lens we have chosen to analyze here, we have selected the radii of curvature of the lens surfaces to reduce spherical aberration. Thus, we see that field curvature aberration forces the locus of foci onto a cylindrical surface, rather than a plane. To access the full field-of-view, the detector array would need to be distributed over the curved surface, an inconvenience since most detector arrays are planar. As in the example of the flattened fish-eye lens, however, the existence of a focal surface can be used to our advantage in the context of TO optimization. We can, for instance, imagine a transformation that will flatten the curved focal surface of the lens to a plane, since the rays terminate anyway on that surface. In so doing, we compensate for the field curvature of the refractive optic by assuming a layer of TO medium placed above the detector plane.

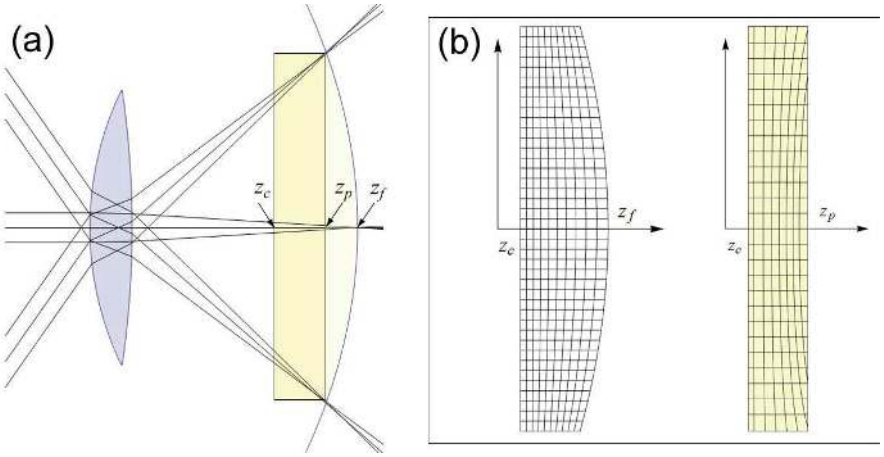

Fig. 6. (a) Ray trace diagram of a refractive lens. The lens causes rays to be focused to an arc, which intersects the optical axis at z_f. The bounded, darker shaded yellow region indicates where the transformation medium will be placed (between z_c and z_p). (b) Transformation and inverse transformation leading to the flattening of the focal surface. The inverse transformation shown compresses the region between the focal arc and z_c to the region between z_c and z_p. The transformation can be used to design a TO device that will effectively flatten the focal surface.

To illustrate the flattening of the focal surface, we first perform a ray trace, as illustrated in Fig. 6a. We then determine the intersection of the rays incident on the focal surface, interpolating to find a curve that describes the shape of the focal surface. We find the focal surface has a parabolic form, described by

$$z = z_0 + a\left(x^2 - b^2\right), \tag{16}$$

where z_0, a and b are constants that are found by fitting the determined locus of focal points. The focal point for rays incident along the optical axis is $z_f = z_0 - ab^2$. We imagine now taking the space that is bounded by the focal surface and a line that lies at some position in front of the focal region, which we designate z_c, and compressing it into the rectangle bounded by z_c and z_p. Such a region is shown as the shaded box in the ray diagram of Fig. 6a. A simple transformation that accomplishes this task is as follows:

#132121 - $15.00 USD Received 23 Jul 2010; revised 14 Sep 2010; accepted 15 Sep 2010; published 22 Sep 2010

$$x' = x$$
$$z' = z + a\left(x^2 - b^2\right)\left(\frac{z - z_c}{z_p - z_c}\right)^2, \tag{17}$$

The transformation defined by Eq. (17), represented by the grids presented in Fig. 6b, gradually expands the rectangular region lying between $z = z_c$ and $z = z_p$ in a manner such that the boundary of the transformed space coincides with the curved focal surface of the lens. Applying the transformation to the rays propagating in the region $z_c \le z \le z_f$, we see that the locus of focal points now has been flattened to that of a plane, at which a planar detector array could be placed. The medium defined by the transformation of Eq. (17) effectively compensates for the field curvature, eliminating one source of aberration. Note that, as before, the medium defined by the grid corresponding to the transformation of Eq. (17) will be generally inhomogeneous and anisotropic, but can be simplified through QCTO transformations.

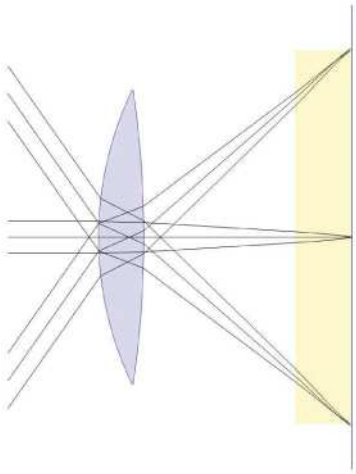

Fig. 7. A compensated refractive lens. The medium in the shaded rectangle is assumed to be derived from the transformation shown in Eq. (17).

The use of transformation optics to compensate field curvature associated with other optical elements provides an alternative means of achieving large field-of-view imaging systems, provided the appropriate medium can be fabricated at the wavelengths of interest. For the case we have shown, we have assumed a conventional refractive bi-convex refractive lens. Note that the process of flattening can be expected to introduce some non-lossy distortion into the image; aberrations due to such distortion can easily be compensated through the use of an appropriate, compensating transformation, as was suggested for the flattening of the Luneburg lens in [13].

5. Conclusion

The examples we have presented are two-dimensional optical devices, valid for waves polarized out-of-plane and propagating within the plane. While the applicability of general TO methods is not restricted in any way to two-dimensional geometries, the QCTO methods that lead to the more realizable material parameters are inherently two-dimensional; there is no simple extension of the QCTO optimization to three dimensions. One might consider simply rotating the index distribution obtained in a QCTO optimization around the optical axis to form a three dimensional structure—a technique that has been applied recently in the demonstration of an optical ground plane cloak [19]. Simulations of a three-dimensional fish-

#132121 - $15.00 USD Received 23 Jul 2010; revised 14 Sep 2010; accepted 15 Sep 2010; published 22 Sep 2010

eye obtained by taking the index distribution in Fig. 4b and rotating it to form a cylinder are shown in Fig. 8. While on-axis rays are brought to a focus, the off-axis rays are considerably distorted, with the solution of Fig. 5 not apparent.

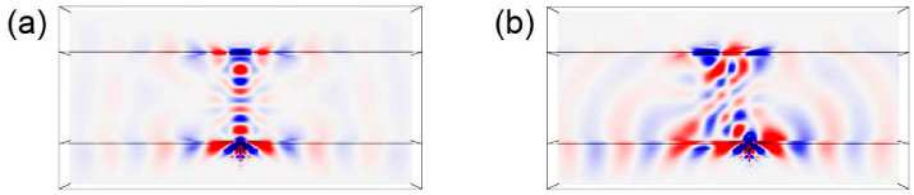

Fig. 8. The three-dimensional generalization of the flattened fish-eye lens obtained by axisymmetric revolution of the index distribution around the optical axis. Full-wave simulation with an electric point dipole source is shown. The free-space wavelength is 0.6*a*, where *a* is the lens thickness. (a) The source (vertically-oriented electric point dipole) is on the optical axis. (b) The source is shifted off-axis by 0.25*a*.

Though the simple approach we have attempted in Fig. 8 fails for isotropic dielectric media, it may yet be possible to achieve three-dimensional QCTO media with somewhat more complicated but achievable material parameters. The optical devices described here and elsewhere clearly reveal the advantages that true three-dimensional QCTO could bring to imaging systems.

Acknowledgments

This work was supported by the Army Research Office through a Multidisciplinary University Research Initiative (MURI), Grant No. W911NF-09-1-0539.

#132121 - $15.00 USD Received 23 Jul 2010; revised 14 Sep 2010; accepted 15 Sep 2010; published 22 Sep 2010